



HAL
open science

An Effective Algorithm for Finding Shortest Paths in Tubular Spaces

Dang Viet Anh Nguyen, Jérôme Szewczyk, Kanty Rabenorosoa

► **To cite this version:**

Dang Viet Anh Nguyen, Jérôme Szewczyk, Kanty Rabenorosoa. An Effective Algorithm for Finding Shortest Paths in Tubular Spaces. *Algorithms*, 2022, 15 (3), 10.3390/a15030079 . hal-04273618

HAL Id: hal-04273618

<https://hal.science/hal-04273618v1>

Submitted on 7 Nov 2023

HAL is a multi-disciplinary open access archive for the deposit and dissemination of scientific research documents, whether they are published or not. The documents may come from teaching and research institutions in France or abroad, or from public or private research centers.

L'archive ouverte pluridisciplinaire **HAL**, est destinée au dépôt et à la diffusion de documents scientifiques de niveau recherche, publiés ou non, émanant des établissements d'enseignement et de recherche français ou étrangers, des laboratoires publics ou privés.

An effective algorithm for finding shortest paths in tubular spaces

Dang-Viet-Anh Nguyen ^{1,*} , Jérôme Szewczyk ² and Kanty Rabenorosa ¹ 

¹ FEMTO-ST Institute, Univ. Bourgogne Franche-Comté, CNRS, 25000 Besançon, France; rkanty@femto-st.fr

² Institute for Intelligent Systems and Robotics (ISIR), Sorbonne University, CNRS, 75005 Paris, France; szewczyk@isir.upmc.fr

* Correspondence: dang.nguyen@femto-st.fr

Abstract: We propose a novel algorithm for Euclidean shortest path (ESP) from a given point (source) to another point (destination) inside a tubular space. The method is based on the observation data of a virtual particle (VP) assumed to move along this path. In the first step, the geometric properties of the shortest path inside the considered space are presented and proven. Utilizing these properties, the desired ESP can be segmented into three partitions depending on the visibility of the VP. Our algorithm will check which partition the VP is belong to and calculate its correct direction of the movement, thus the shortest path will be traced. The proposed method is then compared to Dijkstra's algorithm considering different types of tubular spaces. For all cases, the solution provided by the proposed algorithm is smoother, shorter, and high accuracy with a faster calculation speed than one obtained by Dijkstra's method.

Keywords: Euclidean shortest path; tubular space; reactive algorithm; visibility; oriented drilling process; Dijkstra's algorithm

1. Introduction

Finding the shortest path in the presence of obstacles, referred to as the Euclidean shortest path problem is one of the fundamental problems in path planning [1]. This problem arises in many industrial ^{c1} applications. ^{c2} ^{c3}The idea of using a flying robot such as an unmanned aerial vehicle (UAV) to navigate through a tunnel-like environment can be found in the inspection of dam penstocks, [2–4], chimneys [5], ventilation systems [6], onshore oil and gas industry [7], narrow sewers [8], and other hazardous deep tunnels [9,10]. In addition, many marine applications also require navigating through underwater tunnel-like environments with autonomous underwater vehicles (AUVs). For instance, the inspection of different kinds of underwater structures such as offshore oil platforms [11], flooded spring tunnels [12,13], water delivery tunnels [14], etc. In these applications, shortest path planning that minimizes the total distance travelled by the vehicles plays an important role in optimizing the energy consumption, thus extending the operation time without recharging their batteries [15,16]. It may also reduce the travelling time and will be very useful for search & rescue missions during disaster events in underground tunnels [17,18].

^{c4}Another example of the studied problem is to determine the location of a non-elastic chord between to points within a tube. Indeed, this problem can be found in controlling the deformation of slender tube-like robots actuated with an internal tendon(s) [19,20]. Calculating the tendon load effect on the tube wall requires determining the tendon location. As it is only attached at the tip, pre-positioned at the base, and the rest freely locates inside

Citation: Nguyen, D.V.A.; Szewczyk, J.; Rabenorosa, K. An effective algorithm for finding shortest paths in tubular spaces. *Algorithms* **2022**, *1*, 0. <https://doi.org/>

Received:

Accepted:

Published:

Publisher's Note: MDPI stays neutral with regard to jurisdictional claims in published maps and institutional affiliations.

Copyright: © 2023 by the authors. Submitted to *Algorithms* for possible open access publication under the terms and conditions of the Creative Commons Attribution (CC BY) license (<https://creativecommons.org/licenses/by/4.0/>).

^{c1} ~~Removed text: and medical~~

^{c2} ~~Removed text: In the industry, the~~

^{c3} Text added.

^{c4} Text added.

the innermost tube, its location results in the shortest path connecting two points at the base and at the tip.

1.1. Related works

In general 3D space, the problem of finding the ESP between two given points that does not intersect given obstacles is known to be NP-hard [21], special cases of the problem have been studied afterwards. The author in [22] gave a polynomial time algorithm to calculate ESP for cases where the number of obstacles is ‘small’ and all of them are convex. Another algorithm was proposed in [23] with the assumption that all obstacles are vertical buildings with k different heights. More recently, [24] presented algorithms for solving approximate ESPs amid convex obstacles. Other approximation algorithms for ESP calculations are detailed in [25]. These studies share common features that a collection of finite obstacles are given as forbidden zones in space and the ESP will be found in the space surrounding these obstacles.

In the studied problem, the obstacle is the entire space outside the tube and the ESP must pass through the inner zone of the tubular space. A similar problem can be found in [26] that compute the minimal path in tubular space. The minimal path is typically solved based on the Fast Marching method which only considers grid nodes as the possible vertices of the minimal paths. However, paths detected by the Fast Marching method have been proven to be not always the exact ESPs [1]. There also exist several approximation algorithms for finding ESP between two points in 3D space bounded by a closed surface such as a cube-curves [27] or a simple polyhedron [28] using rubberband algorithm. This method is suitable for solving various ESPs in 3D space. Even so, there is a non-trivial gap in geometric shape between the cube-curve and the tubular space. Polyhedron seems like a better choice to represent a tubular space. However, characteristic geometrical properties of tubular spaces should be considered for a dedicated algorithm.

The studies on tubular surface with Bishop frame was proposed in [29]. The authors gave some characterizations about special curves lying on this surface (e.g., geodesic and asymptotic curves). However, the problem we study requires considering the interior space instead of just the boundary surface. In addition, the geometrical properties of the ESP inside the tubular space also need to be investigated. The authors in [30] described a simple geometric structure of ESPs where they consist of curved paths on the obstacles connected by straight line segments (see Theorem 1). In this work, we develop the geometric structure of ESPs presented in [30] by considering characteristic properties of tubular spaces.

In practice, the navigation problem can be classified into planning-based and reactive algorithms [31]. Planning-based approaches require a global map representation of the environment (e.g., a graph or a network) before searching. The knowledge beforehand of the tubular space allows generating a weighted graph where the weight of each edge (or arc for the directed graph) associated with its length [25]. Numerous algorithms are used for shortest path calculation in graph theory (see Chapter 24 and 25 in [32]). A well-known graph-based algorithm among them is Dijkstra’s algorithm [33] where the shortest path connects vertices in the graph. Unlike the planning-based approaches, a reactive method allows directly generating motion decisions during the movement based on observed data [31]. The reactive shortest path navigation was presented in [34] for an in-plane problem. Such a problem was also found in 3D space where the obtained path is interpolated with a spline curve [35]. In this work, we propose an algorithm that based on the observed information of a virtual particle and can be used as a reactive method for the shortest path navigation inside the tubular space.

1.2. Contributions

In this paper, we propose a novel algorithm to find the shortest path within a tubular space that connects two points at the tube ends. Our contributions include: 1) the description of the ESP geometrical structure inside tubular spaces with mathematical proof, 2) the proposition of a novel algorithm for finding the shortest path in tubular spaces based on

the observed data, and 3) the numerical validation and comparison results with Dijkstra's algorithm by considering various types of tubular spaces. As a result, the solution obtained by using the proposed algorithm is shorter, smoother and faster than one provided by Dijkstra's method.

The remainder of this paper is organized as follows. Section 2 formulates the problem. The basics of Dijkstra's algorithm is described in Section 3. Then, we present the proposed algorithm in Section 4. Our computational results is given in Section 5. After that, Section 6 includes some brief discussions. Section 7 concludes the paper.

2. ESP in Tubular Space

2.1. Problem description

Euclidean geometry is the geometry in daily life [1] where the distance between two points $\mathbf{p} = (x_p, y_p, z_p)^T$ and $\mathbf{q} = (x_q, y_q, z_q)^T$ in 3D space is defined as follows:

$$d_e(\mathbf{p}, \mathbf{q}) = \sqrt{(x_p - x_q)^2 + (y_p - y_q)^2 + (z_p - z_q)^2} \quad (1)$$

From the discrete point of view, a path (α) from the source \mathfrak{P} to the destination \mathfrak{Q} is a finite sequence of nodes \mathbf{x}_i , starting at \mathfrak{P} and ending at \mathfrak{Q} . We obtain the length of the path as in Eq. 2:

$$L(\alpha) = \sum_{i=0}^{n-1} d_e(\mathbf{x}_i, \mathbf{x}_{i+1}), \quad \mathbf{x}_0 = \mathfrak{P}, \mathbf{x}_n = \mathfrak{Q} \quad (2)$$

Then, the ^{c1} ESP is the path connecting \mathfrak{P} and \mathfrak{Q} , which has the minimum length and has to be through a given tubular space. The mathematical definition of tubular space is given as follows [36]:

Definition 1. Let $\mathbf{c}(s) : I \rightarrow \mathbb{R}^3$ be a smooth, regular space curve. A tubular surface $\partial\Omega$ associated to $\mathbf{c}(s)$, of radius ρ , is, by definition, the envelope of the family of spheres of radius ρ , with the center on the curve.

Definition 2. The storage space of the tube Ω is the 3D space enclosed by the lateral wall ($\partial\Omega$) and the two ending cross-sections of the tube.

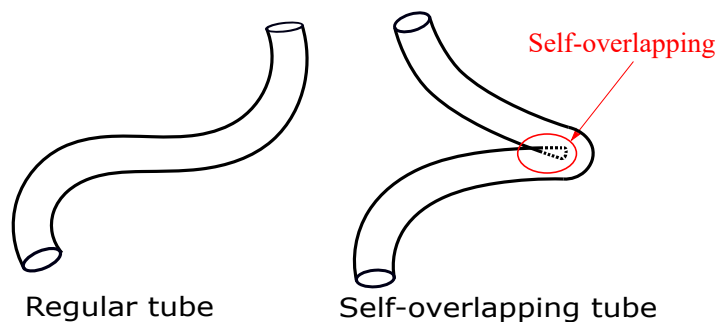


Figure 1. Regular and self-overlapping tube as defined in [29]. The regular tube ensures the correctness of the directed graph in the following section.

^{c2} ^{c3} In Definition 1, s is the arc length parameter of the centerline curve. We consider in this work the tubular surface $\partial\Omega$ to be regular (Fig. 1). The condition underlying the regularity of a tube is given in details in [29]. By $\kappa(s)$, we denote the curvature of the centerline curve

^{c1} Removed text: searching

^{c2} Removed text: where

^{c3} Text added.

$c(s)$. In order to avoid singularities as well as self-overlapping, the following condition is required:

$$\kappa(s) < \rho^{-1}, \forall s \in [0, L] \quad (3)$$

where L is the length of $c(s)$.

2.2. Directed graph

We discretize Ω into a series of meshed circular disks corresponding to the cross-sections perpendicular to $c(s)$. By S_0, \dots, S_{N+1} we denote the meshed circular disks where S_0 contains the starting point (source) \mathfrak{P} and S_{N+1} includes the destination \mathfrak{Q} . The distance between two consecutive disks along the centerline curve is $h = \frac{L}{N+1}$. As the shortest path from the source to the destination must obviously pass through each cross-section at only one point, we have the weighted directed graph $G(V, A)$ as shown in Fig. 2. This directed graph is defined by a finite set V of vertices and a set A of arcs between those vertices [1]. All vertices of the graph (except \mathfrak{P} and \mathfrak{Q}) are located at the nodes of the meshed disks S_1, \dots, S_N . We define that two vertices are called adjacent if they are connected by one arc. Then, every two adjacent nodes in the graph are located on two consecutive disks. The source \mathfrak{P} is connected with all nodes of disk S_1 . Each node of disk S_i is connected by one arc to every node of disk S_{i+1} for all $i \in \{1, \dots, N-1\}$. Eventually, every node of disk S_N is connected directly to the destination \mathfrak{Q} .

3. Basics of Dijkstra's Algorithm

^{c1} The concept of this method, based on the lemma about the relationship between global minimum and local minimum, was first presented by E.W. Dijkstra in 1959 (see [33], Problem 2). ^{c2} Although also based on Lemma 1, Algorithm 1 ^{c3} applied for the directed graph has a run time in $O(|A|)$ instead of $O(|V|\log|V| + |A|)$ like the conventional Dijkstra's algorithm used for a weighted graph in general [1].

Lemma 1. (Dijkstra algorithm, 1959) "If r is a node on the minimal path from p to q , knowledge of the latter implies the knowledge of the minimal path from p to r ".

This lemma can be proved easily by contradiction. The shortest path from the source \mathfrak{P} to the destination \mathfrak{Q} will be traced by extending all extendable paths by one edge to a node not yet visited on this path until \mathfrak{Q} is reached. Consequently, extending all the extendable paths from the source by one arc in the directed graph becomes turning the

^{c1} Remove text: Dijkstra's algorithm solves the problem of finding the shortest path between a point (source) and any other point (destination) in a given graph.

^{c2} Text added.

^{c3} Text added.

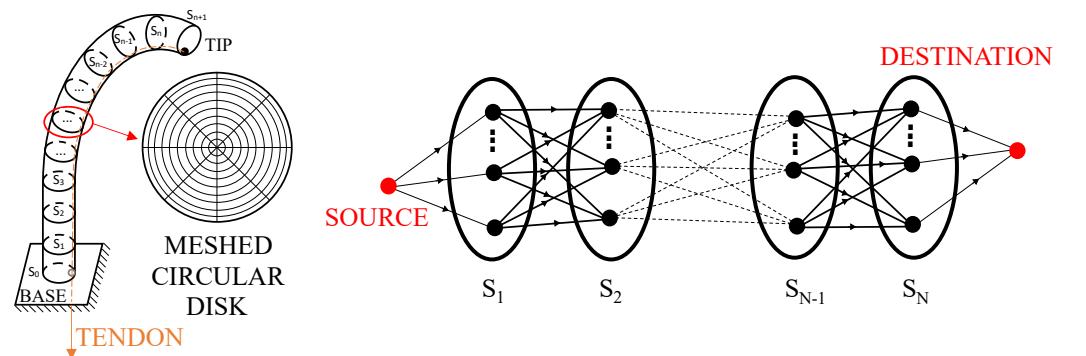


Figure 2. Discrete approach for the ESP problem. (Left): Inner space of the tube transformed into a series of meshed circular disks and (Right): the directed graph.

Algorithm 1: Dijkstra's algorithm

```

Input:  $\mathfrak{P}, \mathfrak{Q}$ , and  $\mathbf{r}_{[i][j]}, \forall i \in \{1, \dots, N\}, \forall j \in \{1, \dots, M\}$ .
Output:  $\mathcal{L}_{[\mathfrak{Q}]}$ .
// Initialisation
1  $D(\mathfrak{Q}) \leftarrow +\infty, D(\mathbf{r}_{[i][j]}) \leftarrow +\infty, \forall i \in \{1, \dots, N\}, \forall j \in \{1, \dots, M\}$ ;
// From the source to  $S_1$ 
2 for  $j \leftarrow 1$  to  $M$  do
3    $D(\mathbf{r}_{[1][j]}) \leftarrow w(\mathfrak{P}, \mathbf{r}_{[1][j]})$ ;
4    $\mathcal{L}_{[1][j]} \leftarrow \{\mathfrak{P}, \mathbf{r}_{[1][j]}\}$ ;
5 end
// Between  $S_1$  and  $S_N$ 
6 for  $i = 2$  to  $N$  do
7   for  $j = 1$  to  $M$  do
8     for  $k = 1$  to  $M$  do
9        $D(\mathbf{r}_{[i][j]}) \leftarrow \min\{D(\mathbf{r}_{[i][j]}), D(\mathbf{r}_{[i-1][k]}) + w(\mathbf{r}_{[i-1][k]}, \mathbf{r}_{[i][j]})\}$ 
10      If  $D(\mathbf{r}_{[i][j]})$  is replaced, put a label  $K^* \leftarrow k$ .
11     end
12      $\mathcal{L}_{[i][j]} \leftarrow [\mathcal{L}_{[i-1][K^*]}, \mathbf{r}_{[i][j]}]$ ; // add  $\mathbf{r}_{[i][j]}$  to the list  $\mathcal{L}_{[i-1][K^*]}$ 
13   end
14 end
// From  $S_N$  to the destination
15 for  $k = 1$  to  $M$  do
16    $D(\mathfrak{Q}) \leftarrow \min\{D(\mathfrak{Q}), D(\mathbf{r}_{[N][k]}) + w(\mathbf{r}_{[N][k]}, \mathfrak{Q})\}$ .
17   If  $D(\mathfrak{Q})$  is replaced, put a label  $K^* \leftarrow k$ .
18 end
19 return  $\mathcal{L}_{[\mathfrak{Q}]} \leftarrow [\mathcal{L}_{[N][K^*]}, \mathfrak{Q}]$ 

```

examined disk into its adjacent disk towards the destination. Once examining a disk, the shortest path between the source and every node on the previous disks has been identified, so we do not need to revisit these points.

Set $\mathbf{r}_{[i][j]} (i \in \{1, \dots, N\}, j \in \{1, \dots, M\})$ be the node j^{th} on the meshed disk S_i . In addition, we denote $D(\mathbf{x})$ as the minimum length from node \mathfrak{P} to node \mathbf{x} , $w(\mathbf{x}, \mathbf{y})$ as the length of the arc connecting two adjacent nodes \mathbf{x} and \mathbf{y} , and $\mathcal{L}_{[i][j]}$ as the list of the nodes on the shortest path from the source \mathfrak{P} to node $\mathbf{r}_{[i][j]}$ (for node \mathfrak{Q} , we utilize $\mathcal{L}_{[\mathfrak{Q}]}$). We obtain Dijkstra's algorithm applied for this ESP problem as given in Algorithm 1.

^{c1}During the operation, all currently visited nodes always belong to the same cross-section. Thus, all possible paths will reach the destination at the same time. When the destination is reached, there will be no longer extendable paths in the directed graph and we can point out the shortest path. For that reason, the algorithm becomes a breadth-first search algorithm [1]. ^{c2}Thus, the time complexity of ^{c3} Algorithm 1 is $O(|A|)$ with $|A|$ is the number of arcs in the directed graph. As a conventional method, the solution by Dijkstra's algorithm is given as a series of vertices of the graph G . Then, the solution path obtained is generally a polyline. To increase the accuracy of the result as well as make it smoother, the mesh of the discretized cross-section must be finer. However, increasing the number of nodes on the mesh results in significantly slowing down the calculation speed. We then proposed a new method that takes atage of the geometrical properties of tubular spaces to improve the searching solution.

^{c1} Text added.

^{c2} Text added.

^{c3} Remove text: the

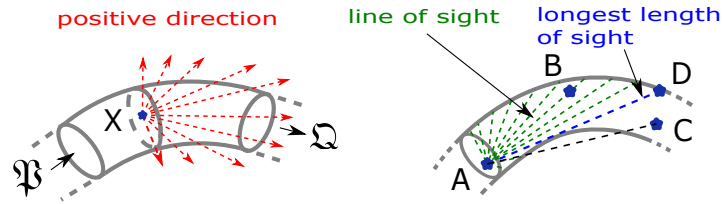


Figure 3. (Left): The dashed red rays describe the positive directions. (Right): A can see B and D because the line segments AB and AD are totally contained by Ω . Also by this definition, A cannot see C . The green and blue dashed lines terminating at the boundary $\partial\Omega$ illustrate the line of sights. Among them, the blue one is the longest-length-of-sight, an important concept used in the following method.

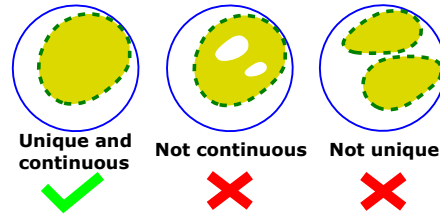


Figure 4. The visible area of a cross-section S_i is described by the yellow zone(s) which must be unique and continuous.

4. The ESP Searching Algorithm Based on Visibility 161

The algorithm we propose hereafter ^{c1}is based on a visible tube portion that can be "seen" by the VP moving along the searching shortest path. The ESP will be gradually figure our by determining the correct moving direction of the particle from the source \mathfrak{P} to the destination Ω . For convenience, we firstly define some concepts used in this section. 162
163
164
165

4.1. Geometric properties of the ESP in tubular space 166

Definition 3. For every point $X \in S_i \subset \Omega$, $i \neq N + 1$, the cross-section S_i divides Ω into 2 sub-spaces, a direction from X is said to be positive (+) if it is towards the sub-space containing the destination. 167
168
169
170

According to Definition 3, any point in Ω (not belonging to S_{N+1}) will have an infinite number of positive directions (see Fig. 3). Obviously, during the movement, the correct direction of the particle is always a positive direction. 171
172
173
174

Definition 4. Two points $X, Y \in \Omega$ are said to see each other if the line segment joining them \overline{XY} is totally contained by Ω . 175
176
177

Definition 5. A cross-section $S \subset \Omega$ is visible from a point $X \in \Omega$ if there exists a point $Y \in S$ that can be seen by X . 178
179
180

Lemma 2. If a point X inside the tube can see a cross-section S of the tube, the area part in S that can be seen by X must be a convex set (as illustrated in Fig. 4). 181
182
183

The proof of this lemma is detailed in the Appendix A.1. 184
185

Definition 6. From a point $X \in \Omega$, the "length of sight" corresponding to a positive direction is the distance between X and the farthest point in $\partial\Omega$ that can be seen by X along the positive direction. The line segment corresponding to this length is called the *line of sight*. 186
187
188
189

^{c1} Text added.

We then have the geometric structure of the shortest path between two points (not see each other) in a tubular space.

Theorem 1. By f , we denote the shortest path between two arbitrary points \mathbf{X} and \mathbf{Y} inside the tubular space Ω . If \mathbf{X} cannot see \mathbf{Y} , then there exist curved parts of f lying on the inner lateral wall of the tube $\partial\Omega$. Outside these parts, f consists of a union of straight line segments which are tangent to the boundary surface $\partial\Omega$.

Theorem 2. The curved parts of f are geodesic paths on $\partial\Omega$. Moreover, they are on the surface of negative curvature.

Proof: The proof of Theorem 1 was presented in [30]. To prove Theorem 2, we employ Lemma 1. As the curved parts of f are also the shortest paths connecting their ends, they must be geodesic paths on the boundary surface $\partial\Omega$ [37]. Moreover, if there exists a curved path of f that is outside the surface of negative curvature, we always find on this path two neighboring points that can see each other (see Fig. 5). As the straight line segment joining these points is shorter than the geodesic path between them, then f is not the shortest one connecting \mathbf{X} and \mathbf{Y} . This contradicts the definition of f (Q.E.D.).

These two theorems lead us to two important corollaries.

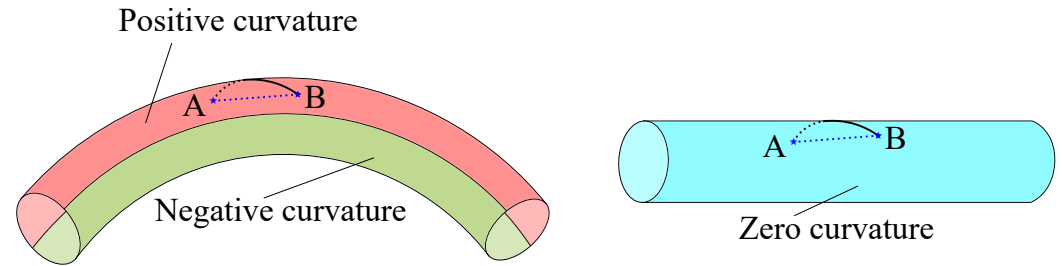


Figure 5. Curved segments lying on surfaces of positive and zero curvatures where A and B can see each other.

Corollary 1. Let \mathbf{X} be a point on the ESP $\mathbf{p}(s)$ that can see a point \mathbf{Y} so that the ray \mathbf{XY} is not the direction $\dot{\mathbf{p}}(s_X)$ of the ESP at \mathbf{X} . Let (α) be an arbitrary plane containing \mathbf{XY} . If the angle between $\dot{\mathbf{p}}(s_X)$ and (α) is not zero, then the direction $\dot{\mathbf{p}}(s)$ at any point on the ESP segment between the cross-sections containing \mathbf{X} and \mathbf{Y} will always point away from (α) .

Proof: From \mathbf{X} , the particle moves away from (α) (the angle between $\dot{\mathbf{p}}(s_X)$ and (α) is not zero). Using Theorem 1, we obtain that the particle only changes its direction at points on the geodesic paths. As these curves must be on surface of negative curvature (Theorem 2) where vector $\dot{\mathbf{p}}(s)$ points out of the tube, thus the $\dot{\mathbf{p}}(s)$ will always point away from the plane (α) (see Fig. 6).

Corollary 2. If \mathbf{X} on the ESP can see a cross-section S of the tubular space Ω via a positive direction, the correct direction at \mathbf{X} ($\dot{\mathbf{p}}(s_X)$) must be towards a point \mathbf{Y} in the visible area of S by \mathbf{X} .

Proof: The above corollary can be proved by contradiction. By $\sigma_X(S)$, we denote the visible area of the cross-section S by \mathbf{X} . Let \mathbf{Y} be the intersection of the straight line containing $\dot{\mathbf{p}}(s_X)$ and the plane containing S (denoted by $\beta(S)$). We need to prove that $\mathbf{Y} \in \sigma_X(S)$. We consider the following hypothesis of contradiction:

$$\text{if } \mathbf{Y} \notin \sigma_X(S) \Rightarrow \overline{\mathbf{XY}} \not\subset \Omega \quad (4)$$

In other words, the ray \mathbf{XY} passes through the boundary $\partial\Omega$. Let \mathbf{M} be the passing point that is closest to \mathbf{X} . In $\beta(S)$ and through \mathbf{Y} , we draw an arbitrary straight line that intersects

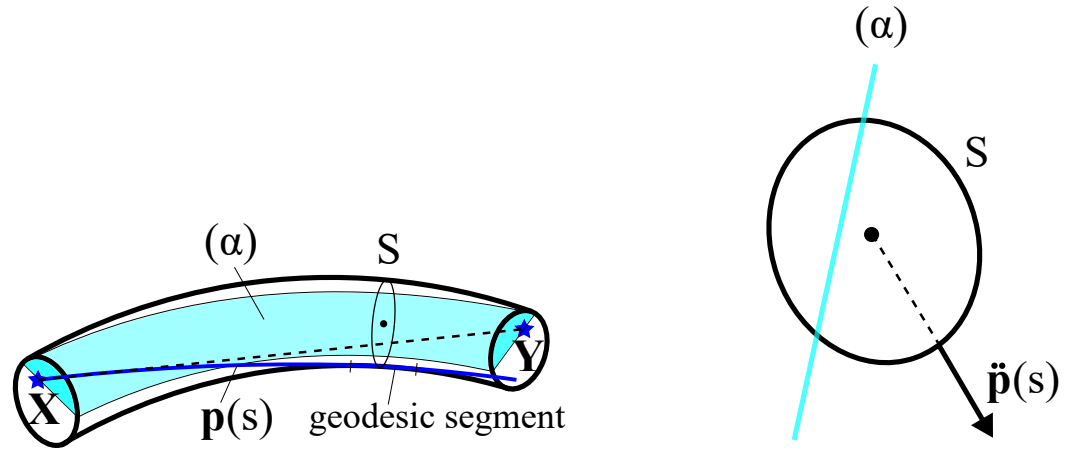


Figure 6. (Left) Tube portion between the cross-sections containing \mathbf{X} and \mathbf{Y} which can see each other. (α) is an arbitrary plane containing \mathbf{XY} but not containing $\dot{\mathbf{p}}(s_X)$. The ESP $\mathbf{p}(s)$ only changes its direction $\dot{\mathbf{p}}(s)$ on its geodesic segment(s). S is an arbitrary cross-section of the tube where the geodesic segment crosses. (Right) On the projection view plane that is perpendicular to (α) ((α) degenerates to a straight line), as $\dot{\mathbf{p}}(s)$ points outside the envelope of S , it also points away from (α) . As $\dot{\mathbf{p}}(s_X)$ points away from (α) , by mathematical induction $\dot{\mathbf{p}}(s)$ will point away from (α) , $\forall s \in [s_X, s_Y]$.

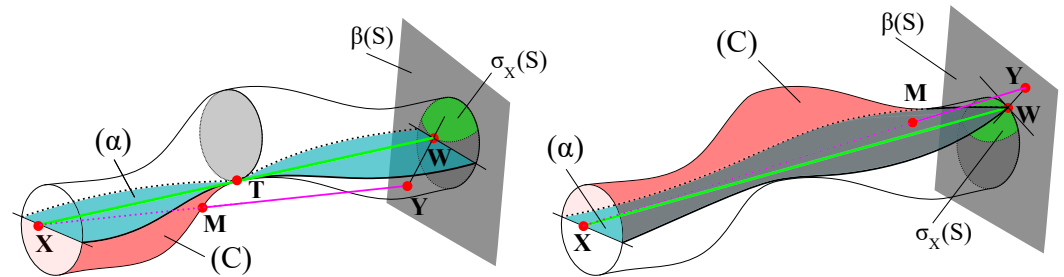


Figure 7. Point \mathbf{X} can see cross-section S . \mathbf{Y} be the intersection of the direction of the ESP $\dot{\mathbf{p}}(S_X)$ and the plane containing S . In $\beta(S)$ and through \mathbf{Y} , we draw an arbitrary straight line that intersects the visible area $\sigma_X(S)$. Let \mathbf{W} be the intersection point that is closest to \mathbf{Y} . (Left): \mathbf{W} is in the inner zone of S . (Right): \mathbf{W} is on the boundary of S .

the visible area $\sigma_X(S)$. Let \mathbf{W} be the intersection point that is closest to \mathbf{Y} . Then, \mathbf{W} must be on the boundary of $\sigma_X(S)$ (denoted by $\partial\sigma_X(S)$). In addition, there is a total of two relative positions of \mathbf{W} : $\mathbf{W} \in \partial\Omega$ and $\mathbf{W} \notin \partial\Omega$ (see Fig. 7). In the following, we define a plane (α) and a closed surface (C) for these two mentioned cases:

- ($\mathbf{W} \notin \partial\Omega$). (α) is the plane that contains \mathbf{XW} and the tangent at \mathbf{W} of $\sigma_X(S)$. If $\overline{\mathbf{XW}}$ is not tangent to $\partial\Omega$, we can always find in $\beta(S)$ a circle with center \mathbf{W} and radius ϵ small enough so that the entire circle can be seen by \mathbf{X} (as there is no obstacle between \mathbf{X} and this circle). Then there exist points outside $\sigma_X(S)$ (which is part of the circle) that can be seen by \mathbf{X} . This contradicts the definition of $\sigma_X(S)$. Thus $\overline{\mathbf{XW}}$ is tangent to $\partial\Omega$. Let \mathbf{T} be the tangent point that is closest to \mathbf{X} and $P_T(\partial\Omega)$ be the tangent plane of $\partial\Omega$ at \mathbf{T} . If $P_T(\partial\Omega) \neq (\alpha)$, $P_T(\partial\Omega)$ will divide $\sigma_X(S)$ into two subsets. However, as the line of sight of a visible point in $\sigma_X(S)$ must pass through the cross-section at \mathbf{T} of the tube, then only one subset of $\sigma_X(S)$ can be observed by \mathbf{X} . This contradicts the definition of $\sigma_X(S)$. Thus, $P_T(\partial\Omega) \equiv (\alpha)$. We can then define a closed surface (C) enclosed by (α) , the cross-section at \mathbf{X} , and part of $\partial\Omega$ which contains \mathbf{M} (see Fig. 7 Left).
- ($\mathbf{W} \in \partial\Omega$). (α) is the plane that contains \mathbf{XW} and the tangent at \mathbf{W} of S . Then, (C) is the closed surface containing \mathbf{M} and enclosed by $\partial\Omega$, (α) , and the cross-section at \mathbf{X} of the tube (see Fig. 7 Right).

Algorithm 2: Proposed method

```

Input:  $\mathfrak{P}, \mathfrak{Q}$ , and  $r_{[i][j]}, \forall i \in \{1, \dots, N\}, \forall j \in \{1, \dots, M\}$ .
Output:  $C_i, \forall i \in \{0, \dots, N+1\}$ .
// Initialisation
1  $C_0 \leftarrow \mathfrak{P}, C_{N+1} \leftarrow \mathfrak{Q}, C_i \leftarrow \emptyset, \forall i \in \{1, \dots, N\}$ ;
2  $flag \leftarrow 0$ ; // Marking if the  $C_{i-1}$  can see  $S_{N+1}$  or not
// Loop Process
3 for  $i \leftarrow 1$  to  $N+1$  do
4   if  $C_{i-1}$  can see  $C_{N+1}$  then
5     //  $C_{i-1}$  is belong to Partition 1
6      $C_k \leftarrow \overline{C_{i-1}C_{N+1}} \cap S_k, \forall k \in \{i, \dots, N\}$ ;
7      $flag \leftarrow 1$ ;
8     break;
9   else
10     $\theta \leftarrow +\infty$ ; // Angle between the correct direction and  $\overrightarrow{C_{i-1}\mathfrak{Q}}$ 
11    for  $j \leftarrow 1$  to  $M$  do
12       $C_{distal} \leftarrow r_{[N+1][j]}$ ; // Temporary examined vertex of  $S_{N+1}$ 
13      if  $C_{i-1}$  can see  $C_{Distal}$  then
14         $flag \leftarrow 1$ ; //  $C_{i-1}$  is belong to Partition 2
15         $C_{temp} \leftarrow \overline{C_{i-1}C_{distal}} \cap S_i$ ; // Possible value for  $C_i$ 
16         $\theta_{temp} = Angle(\overrightarrow{C_{i-1}C_{distal}}, \overrightarrow{C_{i-1}\mathfrak{Q}})$ ; // Possible value for  $\theta$ 
17        if  $\theta > \theta_{temp}$  then
18           $\theta \leftarrow \theta_{temp}$ ;
19           $C_i \leftarrow C_{temp}$ ;
20        end
21      end
22    end
23    if  $flag = 0$  then
24      //  $C_{i-1}$  is belong to Partition 3
25       $C_i = \text{Oriented Drilling Process}(C_{i-1})$ ;
26    end
27  end
28 end

```

finding the series of C_i . It is important to note that C_i is not necessarily a node of $G(V, A)$. Indeed, the algorithm figures out the correct direction of C_{i-1} thereby determining the position of C_i as the intersection point between this direction and the next cross-section S_i . The correct direction of C_{i-1} is found using Remark 1 by checking which partition C_{i-1} ^{c1} belongs to (with precedence from P1 to P3). The value 1 of $flag$ marks that C_{i-1} can see the ending cross-section S_{N+1} . The **Oriented Drilling Process** is an algorithm employed for Partition 3, which returns to the next value of C_i series by the intersection point between the longest-length-of-sight direction and the next cross-section. 274
275
276
277
278
279
280
281

4.3. Oriented Drilling Process 282

To determine effectively the longest-length-of-sight from an arbitrary point X inside the tube, we employ Lemma 2. The operation scheme of finding the longest-length-of-sight direction illustrated in Fig. 9 comprises a series of expanding and deepening processes. Without loss of generality, we assume that C_{i-1} can see a point T in a forward section S_j . By employing Lemma 2, we expand discretely the examined direction from the direction passing through T to others passing through its nearby nodes on the same mesh S_j until 283
284
285
286
287
288

^{c1} Remove text: is belong

^{c2} Text added.

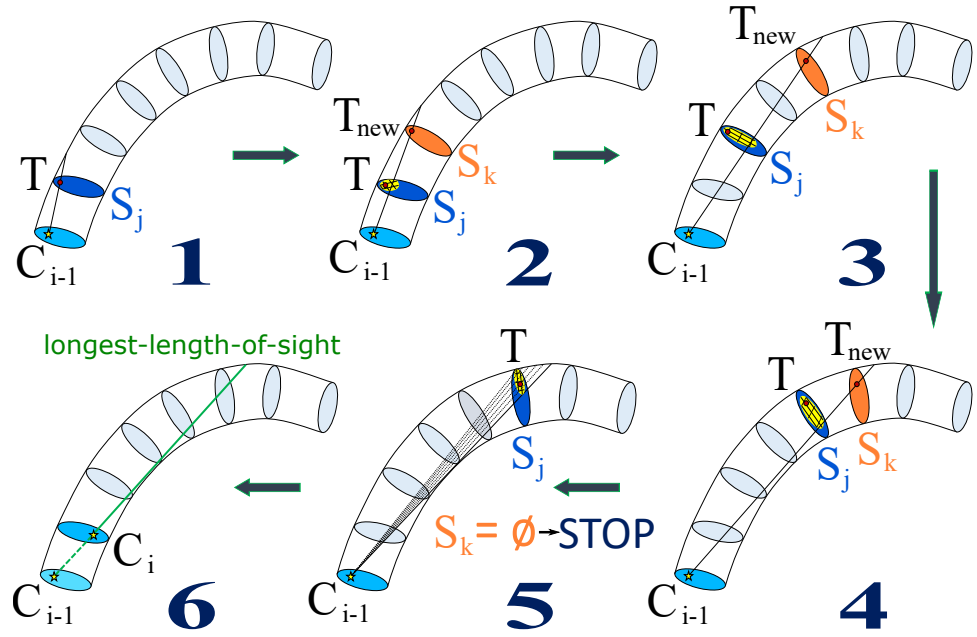
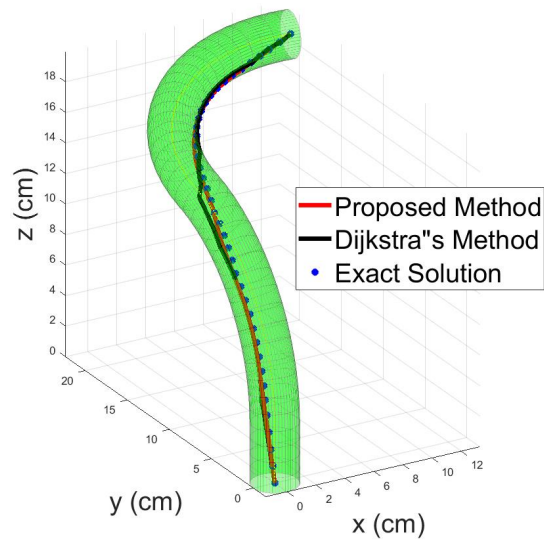


Figure 9. The oriented drilling process : 1) C_{i-1} can see T in section S_j , 2) expand the examined direction in the vicinity of T until seeing T_{new} in section $S_k (k > j)$, 3) update T by T_{new} , S_j by S_k and repeat step 2 for the new T and S_j , 4) repeat step 3, 5) the expanding process is over and we do not find any farther section $S_k = \emptyset$, we then compare all the length of sight passing through the visible area in S_j to obtain the direction corresponding to the longest-length-of-sight, and 6) initialize the next correct point of the shortest path C_i as the intersection point between the correct direction and cross-section S_i .

discovering a point T_{new} in a farther disk $S_k (k > j)$. As a deepening process, we then update T by T_{new} and also the examined cross-section S_j by S_k . The operation is then repeated until the expanding process is over. The condition to stop the expanding process is when the boundary of the visited area in S_j just comprises the invisible nodes and the boundary points of S_j . Finally, we compare the length of sight corresponding to all visible points in farthest visible cross-section and find the longest one. The next correct point C_i is the intersection point between this line of sight and the next cross-section S_i . One atage of this method is a significant improvement in computation time as we do not need to visit all the nodes of the graph. For the expanding process, on the examined disk S_j , we just need to expand the investigated nodes until the current exact point C_{i-1} can see farther, then we jump further into the more in-depth cross-section. Otherwise, if there is no new disk observed by C_{i-1} , we stop the process and indicate the next correct point of the ESP C_i . Moreover, as this is an inheritable algorithm, in the next searching process, we can use directly the previous correct direction as the initial examined orientation. Thus, we skip the disks that were examined in the previous loop. For several circumstances such as points on the straight-line segments of the shortest path (the ESP consists of straight-line and geodesic curve segments, see Theorem 1-2), the next searching process can stop right after choosing this initial examined orientation. That is also the reason why we call this method Oriented Drilling. Imagine that every time we find the correct direction for the point C_{i-1} like we drill a hole in that direction. For the next searching process, as there was already a hole, the searching is much more comfortable. The whole process becomes adjusting the direction of the drill so that it can drill deeper. Consequently, the drilling direction will be oriented closer and closer to the deepest drill hole (the longest-length-of-sight).

5. Computational Results

In this section, we will compare the efficiency of the proposed algorithm with Dijkstra's one. There are several criteria for this comparison result: the length of the obtained ESP, the



L.P = 36.63 (mm), L.D = 37.24 (mm), L.E = 36.59 (mm)

T.P = 759 (ms), T.D = 4103 (ms)

Figure 10. Tubular space with two curved segments in space. By **L.P**, and **T.P**, we denote the tendon length and the computation time for the solution obtained by the proposed method. Similarly, **L.D**, and **T.D** for Dijkstra's algorithm. The exact solution is determined by using Dijkstra's method with $N_\rho = 144$ and $N_\theta = 64$.

computation speed, the smoothness and the position error of the solution. The experiments were ran on a machine with an Intel Core i5-8400 CPU @ 2.80 GHz processor. It has a 6-core CPU and the available RAM was 16 GB. All algorithms were implemented in Matlab.

5.1. Computation Time

We firstly implemented them considering a tube with the centerline in 3D space consisting of a 4 cm straight length and two curved segments belonging to two perpendicular planes. The radii of both curves are 12 cm and their lengths are 16 cm and 20 cm respectively as detailed in Fig. 10. The inner diameter of the tube is 3 cm. We chose the discretization step $h = 2$ mm ($N = 199$). Each meshed disk is made by dividing the cross-section into ^{c1} 25 concentric circles ($N_\rho =$ ^{c3} 25) whose circumference are divided into 4 equal arcs ($N_\theta = 4$).

As shown in Fig. 10, the proposed method allows us to obtain a shorter and smoother solution than Dijkstra's method with the same mesh (detailed analysis will be provided in the next sub-section). Another atage of the proposed algorithm compared to Dijkstra's method is the computation speed as a large number of unimportant vertices and arcs can be ignored in the process (see Fig. 10). As the time complexity of the proposed method has a huge variation depending on the specific shape of the tubular space, the computation time (instead of the theoretical time complexity) will be consider for the comparison result. Table 1 shows how the computation times of the two methods depend on the number of nodes in the meshed circular disks. As we can see the computation time of Dijkstra's method will increase by a factor of 4 if M is doubled (M is the number of nodes in a

^{c1} Remove text: 20

^{c2} Text added.

^{c3} Remove text: 20

^{c4} Text added.

Table 1. Computation Time (in Second) Of The Two Mehods

M = 100	$N_\rho = 25, N_\theta = 4$ T.P = 0.76, T.D = 4.10	
M = 200	$N_\rho = 50, N_\theta = 4$ T.P = 0.96, T.D = 16.66	$N_\rho = 25, N_\theta = 8$ T.P = 1.05, T.D = 15.77
M = 400	$N_\rho = 100, N_\theta = 4$ T.P = 1.63, T.D = 64.67	$N_\rho = 25, N_\theta = 16$ T.P = 1.51, T.D = 60.19
M = 800	$N_\rho = 200, N_\theta = 4$ T.P = 3.03, T.D = 259.23	$N_\rho = 25, N_\theta = 32$ T.P = 2.01, T.D = 219.82

meshed disk). This is consistent with the time complexity $O(|A|)$ of Dijkstra's algorithm ($|A| = 2M + (N - 1)M^2$). For the proposed method, this increasing rate is less than two. 336
337

5.2. Accuracy and smoothness 338

In the following, we extend the comparison results between the two algorithms for different types of tubular spaces as shown in Table 2. Depending on the properties of the centerline, we have two main classes of the tubular spaces: in plane centerline (parabolic, elliptical, hyperbolic, sinusoidal, and evolvent of a circle) and in space centerline (wave-shaped torus on a sphere, helical, spiral, and complex shape). ^{c1}Each meshed disk is chosen with $N_\rho = 25$ and $N_\theta = 4$. In all these cases, the proposed algorithm always gives shorter, smoother and faster results than Dijkstra's algorithm with the same mesh. Unlike conventional graph-based methods (e.g. Dijkstra's searching algorithm) in which the shortest path is made up of the graph nodes, the proposed method allows finding each correct point on the ESP by determining the intersection between the exact moving direction (line of sight) and the next cross-section. This intersection point is not necessary a node of the mesh and leads to a smoother and shorter solution than one by Dijkstra's algorithm. The smoothness of this path is important, especially in mechanical applications when the derivatives of the path with respect to the arc length s of the tube is required such as using the coupled Cosserat rod and string model [38] to find the deformation of a flexible tendon drive robot in case that the tendon locates freely inside the tube [19]. 339
340
341
342
343
344
345
346
347
348
349
350
351
352
353
354

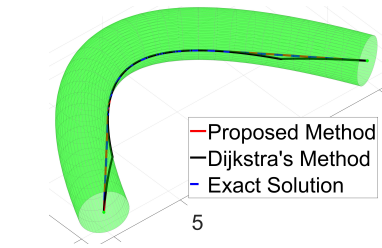
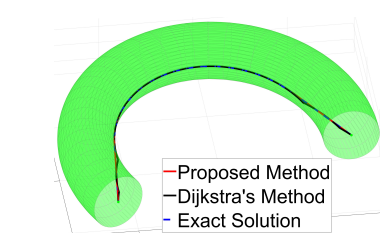
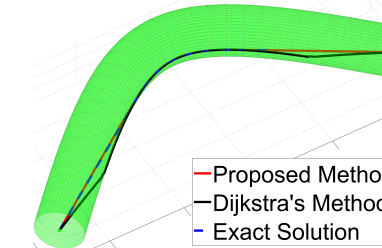
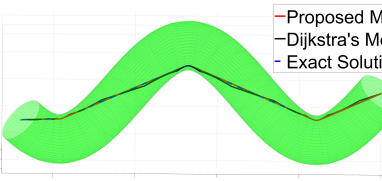
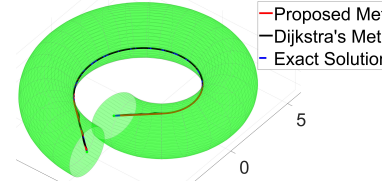
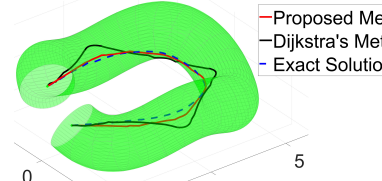
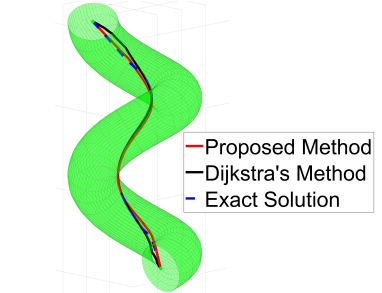
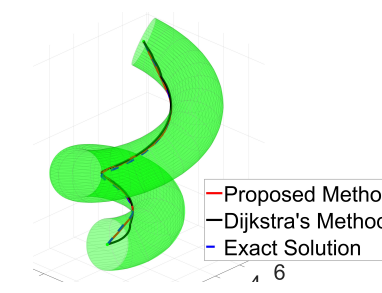
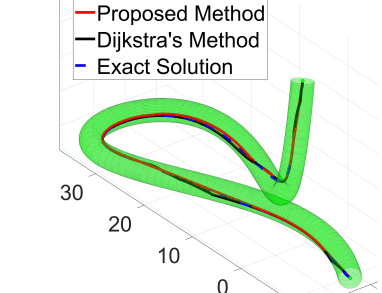
Besides the length and the smoothness of the obtained ESP, its location inside the tube is also very important. For example, in the mechanical problem just mentioned above, the tendon location directly related to the deformation direction of the tube. Thus, the position error of the obtained ESP to the exact solution need to be investigated. We consider the ESPs given by Dijkstra's and the proposed algorithms to be a series of points located on the cross-sections of the tube. Then, the position error of each point is the distance between itself and the exact solution within the containing cross-section. Let ϵ_i^D and ϵ_i^P are the position errors within cross-section S_i of the solution by Dijkstra's algorithm and by the proposed method respectively. In this test, we expect to consider the relative errors instead of the absolute ones. As the obtained paths must be inside the tubular space, to limit the relative errors by 100%, we compare the absolute position error to the inner diameter of the tube d . The root mean square error (RMSE) and the maximum error (E_{max}) of Dijkstra's solution are given in Eq. 5 and Eq. 6 (the same for the proposed method just by replacing super index D by P).

$$RMSE = \frac{1}{d} \sqrt{\frac{1}{N} \sum_{i=1}^N (\epsilon_i)^2} \quad (5)$$

$$E_{max} = \min_{i \in \{1, \dots, N\}} \left(\frac{\epsilon_i}{d} \right) \quad (6)$$

^{c1} Text added.

Table 2. Compare the proposed method and Dijkstra's method with many tubular surfaces [39].

<p>1. Plane Parabolic Centerline</p>  <p>— Proposed Method — Dijkstra's Method — Exact Solution</p> <p>5</p> <p>L.P = 27.22, L.D = 27.29, L.E = 27.21 (cm) T.P = 0.68, T.D = 2.57 (s)</p>	<p>2. Plane Elliptical Centerline</p>  <p>— Proposed Method — Dijkstra's Method — Exact Solution</p> <p>5</p> <p>L.P = 25.70, L.D = 25.74, L.E = 25.68 (cm) T.P = 1.02, T.D = 2.65 (s)</p>	<p>3. Plane Hyperbolic Centerline</p>  <p>— Proposed Method — Dijkstra's Method — Exact Solution</p> <p>5</p> <p>L.P = 27.97, L.D = 28.10, L.E = 27.96 (cm) T.P = 0.73, T.D = 2.64 (s)</p>
<p>4. Plane Sinusoidal Centerline</p>  <p>— Proposed Method — Dijkstra's Method — Exact Solution</p> <p>4</p> <p>L.P = 24.41, L.D = 24.53, L.E = 24.39 T.P = 1.36 (s), T.D = 2.66</p>	<p>5. Plane Evolvent of a Circle</p>  <p>— Proposed Method — Dijkstra's Method — Exact Solution</p> <p>5</p> <p>L.P = 21.92, L.D = 21.94, L.E = 21.91 T.P = 1.16 (s), T.D = 2.57</p>	<p>6. Wave-Shaped Torus on a Sphere</p>  <p>— Proposed Method — Dijkstra's Method — Exact Solution</p> <p>5</p> <p>L.P = 22.29, L.D = 25.12, L.E = 21.96 T.P = 1.26 (s), T.D = 2.74</p>
<p>7. Tubular Helical Surface</p>  <p>— Proposed Method — Dijkstra's Method — Exact Solution</p> <p>6</p> <p>L.P = 20.05, L.D = 20.31, L.E = 20.01 T.P = 1.00 (s), T.D = 2.74</p>	<p>8. Tubular Spiral Surface</p>  <p>— Proposed Method — Dijkstra's Method — Exact Solution</p> <p>6</p> <p>L.P = 18.87, L.D = 19.02, L.E = 18.71 T.P = 1.17 (s), T.D = 2.88</p>	<p>9. Complex Shape Tubular Surface</p>  <p>— Proposed Method — Dijkstra's Method — Exact Solution</p> <p>30</p> <p>L.P = 110.96, L.D = 111.22, L.E = 110.92 T.P = 5.90 (s), T.D = 11.29</p>

Here, we do not consider the two ending cross-sections (S_0 and S_{N+1}) as the position error is obviously zero at the source and the destination. As shown in Table 3, the proposed method always provides smaller $RMSE$ and E_{max} than ones obtained by Dijkstra's algorithm for all of the tubes. Concretely, the average values among these tubes of $RMSE$ and of E_{max} for the proposed solution are respectively 0.319% and 1.427% and about 6 times smaller than ones given by Dijkstra's algorithm (2.133% and 8.753%, respectively). ^{c2}As the path obtained by Dijkstra's method must pass through nodes of the weighted graph, its position errors depend a lot on the meshing. These errors can be reduced if we increase the granularity of the mesh, but it will also increase the computation time. For the proposed method, the location of the obtained path is not forced to be the nodes of the graph that leads to smaller position errors.

^{c2} Text added.

Table 3. Root mean square and maximum position errors of the ESP obtained by the two algorithm. The tube number is as given in Table 2.

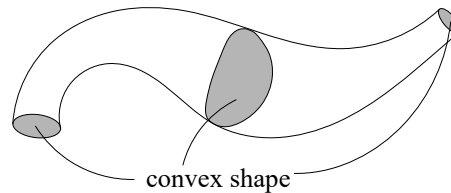
RMSE										
Tube	1	2	3	4	5	6	7	8	9	Avg.
Dijkstra's algorithm	0,506 %	0.032 %	1.922 %	0.118 %	0.007 %	12.487 %	1.655 %	1.334 %	1.140 %	2.133 %
Proposed algorithm	0.002 %	0.002 %	0.004 %	0.009 %	0.001 %	1.003 %	0.510 %	0.368 %	0.974 %	0.319 %
Maximum Error										
Tube	1	2	3	4	5	6	7	8	9	Avg.
Dijkstra's algorithm	4.343 %	0.628 %	11.812 %	1.136 %	0.226 %	28.121 %	8.556 %	11.942 %	12.017 %	8.753 %
Proposed algorithm	0.012 %	0.016 %	0.026 %	0.105 %	0.015 %	4.774 %	2.077 %	2.039 %	3.782 %	1.427 %

6. Discussion 366

In this section, the extended application scope of the proposed algorithm and the ability to apply it as a reactive method for the navigation problem in unknown environments will be discussed. 367
368
369

6.1. Extended Applications 370

We can extend the application scope of the proposed method for general tunnels with convex and variable cross-sections (see Fig. 11). Indeed, with a minor modification on Remark 1 for points in P3: the correct direction is towards the (only) visible point of the farthest visible cross-section instead of considering the longest-length-of-sight, one can confirm that the correctness of Remark 1 will still be preserved (see the Appendix A.2). 371
372
373
374
375

**Figure 11.** Canal space with convex and variable cross-sections.

6.2. A Reactive Method 376

In this work, we used the same directed graph for Dijkstra's algorithm and the proposed one for the aim of simplify the validation and the comparison results. It is important to note that the proposed method does not require the knowledge of the entire volume Ω to obtain a weighted graph before searching. In fact, the correct direction of the particle can be determined based on the observation in front of it. While using Dijkstra's algorithm, we cannot figure out which path is the ESP until visiting all nodes and arcs of the graph and need to store all possible paths during operation, the proposed method allows directly generating motion decision during the movement there by the ESP is gradually traced. Thus, it can be applied as a reactive method for robots that need to explore unknown tubular spaces such as lava tubes on an astronomical object [40] or environments in the absence of GPS signals [41]. In practice, the proposed algorithm should be run together with a given safety boundary constraint for collision avoidance of the inspection robots. 377
378
379
380
381
382
383
384
385
386
387
388

7. Conclusion 389

In this paper, we presented a novel algorithm for solving the ESP problem inside tubular spaces based on its geometric properties. Computational results were conducted on various types of tubular spaces. We demonstrated that the achieved efficiency of the 390
391
392

proposed algorithm is ^{c1} better than Dijkstra's one. Concretely, the proposed method provided smoother and more precise results with a faster calculation speed than one obtained by Dijkstra's algorithm with the same grid. The strength of the proposed method is also reflected in the fact that it can work without knowing the environment in advance which allows it to process as a reactive method. Even though the algorithm was described for the tubular space it is also strongly promising for more complex tunnel spaces, to which it can directly be applied with the mentioned minor modification. ^{c2}A limitation of this method is that it is only applicable to unbranched tubular spaces. In order to apply this method for a branched tubular space, additional information will be required to make decisions at the junctions of branches.

As the ESP may lie on the tubular surface, the requirement of using a collision-free method together with the proposed algorithm has been left for future research. Our plans for future work concern some applications such as on-line trajectory generation of navigation robots in unknown tunnels or determine the deformation of a tendon drive tube-like robot in medical that is also our domain of interest.

Author Contributions: Conceptualization, D.V.A.N. and K.R.; methodology, D.V.A.N. and K.R.; software, D.V.A.N.; validation, D.V.A.N., J.S. and K.R.; mathematical proofs, D.V.A.N, J.S. and K.R.; investigation, D.V.A.N., J.S. and K.R.; resources, D.V.A.N., J.S. and K.R.; data analysis, D.V.A.N., J.S. and K.R.; writing—original draft preparation, D.V.A.N., J.S. and K.R.; writing—review and editing, D.V.A.N., J.S. and K.R.; funding acquisition, J.S. and K.R. All authors have read and agreed to the published version of the manuscript.

Funding: This work was funded by the regional BFC project CoErCIVE, the EIPHI Graduate School (contract "ANR-17-EURE-0002") and ANR μ RoCS (contract "ANR-17-CE19-0005").

Conflicts of Interest: The authors declare no conflict of interest.

Appendix A

Appendix A.1 Proof of Lemma 2

By S_X , we denote the cross-section of Ω that contains \mathbf{X} . Let Ω_m and L_m be the sub-space of Ω limited between S_X and S , and its length along the centerline curve respectively. Under a discrete point of view, Ω_m can be considered as a series of $(K + 1)$ cross-sections perpendicular to the centreline curve: $S_X = S_0^m, \dots, S_K^m = S$ ($K \in \mathbb{N}^+$) with the discrete step $\Delta h = \frac{L}{K}$. Let $\sigma_X(S)$ be the visible area of the cross-section S by \mathbf{X} , we then have:

$$\forall \mathbf{Y} \in \sigma_X(S), \forall i \in \{0, \dots, K\} \Rightarrow \exists \mathbf{a}_i = (\overline{\mathbf{X}\mathbf{Y}} \cap S_i^m) \neq \emptyset$$

Therefore, \mathbf{Y} is the perspective projection of \mathbf{a}_i ($\forall i \in \{0, \dots, K\}$) from the view point \mathbf{X} to the view plane S , hence:

$$\sigma_X(S) \subset \bigcap_{i=0}^K P_X^S(S_i^m)$$

where $P_X^S(S_i^m)$ is the perspective projection of S_i^m from the view point \mathbf{X} to the view plane S . If $K \rightarrow \infty$, or $\Delta h \rightarrow 0$, then, the problem becomes continuous:

$$\sigma_X(S) \subset \bigcap_{i=0}^{\infty} P_X^S(S_i^m) \quad (\text{A1})$$

Inversely,

$$\forall \mathbf{W} \in \bigcap_{i=0}^{\infty} P_X^S(S_i^m) \Rightarrow (\overline{\mathbf{X}\mathbf{W}} \cap S_i^m) = \mathbf{b}_i \neq \emptyset, \forall i \in \mathbb{N} \quad (\text{A2})$$

^{c1} Remove text: much

^{c2} Text added.

When $\Delta h \rightarrow 0$, we then obtain:

$$\overline{\mathbf{XW}} = \bigcup_{i=0}^{\infty} \mathbf{b}_i \subset \Omega$$

Indeed, if $\overline{\mathbf{XW}} \not\subset \Omega$, we can always find a value $\Delta h > 0$ in order to have a cross-section S_i^m so that $S_i^m \cap \overline{\mathbf{XW}} = \emptyset$ (conflict with (A2)). Consequently, \mathbf{W} can be seen by \mathbf{X} , we then have:

$$\mathbf{W} \in \sigma_X(S) \Rightarrow \bigcap_{i=0}^{\infty} P_X^S(S_i^m) \subset \sigma_X(S) \quad (\text{A3})$$

From (A1) and (A3), then:

$$\sigma_X(S) = \bigcap_{i=0}^{\infty} P_X^S(S_i^o) \quad (\text{A4})$$

As the cross-section of Ω is convex and the convexity is preserved under perspective projection and intersection [42], then $\sigma_X(S)$ is a convex region. (Q.E.D.)

Appendix A.2 Proof of Remark 1

^{c1} ^{c2} We will prove the correctness of the proposed direction of the VP at each partition.

i. Case 1: $\mathbf{X} \in \mathbf{P1}$ (\mathbf{X} can see Ω)

As the line segment joining \mathbf{X} and Ω is the shortest path between them. The direction of the ESP $\dot{\mathbf{p}}(s)$ at \mathbf{X} must be towards Ω .

ii. Case 2: $\mathbf{X} \in \mathbf{P2}$ (\mathbf{X} can see S_{end} , but not Ω)

Let $\mathbf{Y} \in \sigma_X(S_{end})$ be the set of visible points on the ending cross-section such that the angle between \mathbf{XY} and $\mathbf{X}\Omega$ is the smallest one. We define a cone surface (C_0) with the apex \mathbf{X} and the generatrix makes an angle $\widehat{\mathbf{YX}\Omega}$ to the axis $\mathbf{X}\Omega$, then $\mathbf{Y} \in (\sigma_X(S_{end}) \cap C_0)$ (see Fig. A1). As $\sigma_X(S_{end})$ is convex, we can easily prove that the existence of \mathbf{Y} is unique, moreover $\mathbf{Y} \in (\partial\sigma_X(S_{end}) \setminus \partial\Omega)$. Thus, \mathbf{XY} must be tangent to $\partial\Omega$ at \mathbf{T} . Let (α) be the corresponding tangent plane, we obtain that (α) is also the tangent plane of $\sigma_X(S_{end})$ (see the proof of Corollary 2 for a similar case).

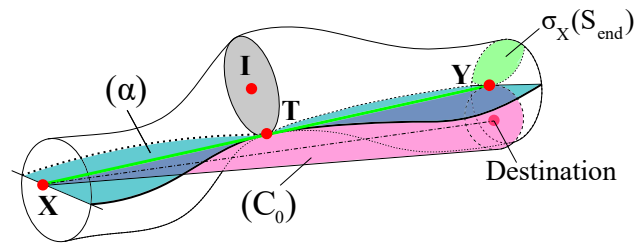


Figure A1. \mathbf{X} can see the ending cross-section. By defining the cone surface (C_0), we can prove that Ω is coplanar with $\mathbf{X}, \mathbf{I}, \mathbf{Y}$.

As \mathbf{Y} is the tangent point between $\sigma_X(S_{end})$ and $(C_0 \cap S_{end})$ (these two convex sets have only one common point \mathbf{Y}), (α) is also the tangent plane of (C_0) . Let \mathbf{I} be the center of the cross-section at \mathbf{T} . As $\mathbf{IT} \perp (\alpha)$, \mathbf{IT} must intersect the axis $\mathbf{X}\Omega$ of (C_0) . Thus, $\mathbf{X}, \mathbf{T}, \mathbf{I}, \mathbf{Y}$, and Ω are coplanar. We denote this coplanar plane by (P_c) .

Let \mathbf{W} be the intersection between the ending cross-section plane $\beta(S_{end})$ and $\dot{\mathbf{p}}(s_X)$. Now, we have to prove that $\mathbf{W} \equiv \mathbf{Y}$. Using Corollary 2, we obtain: $\mathbf{W} \in \sigma_X(S_{end})$. Let (C_1) be the closed surface enclosed by $\sigma_X(S_{end})$ and the set of line segments from \mathbf{X} to every point of $\partial\sigma_X(S_{end})$. Thus, \mathbf{X} can see every point in (C_1) . If $\mathbf{W} \notin \partial\sigma_X(S_{end})$ (that is, \mathbf{W} is belong to the

^{c1} ~~Remove text: It is evident that every point on the ESP must belong to one of the three partitions (P1: see Ω , P2: see S_{end} , but not see Ω , and P3: not see S_{end}). Then, we need to~~

^{c2} Text added.

inner zone of $\sigma_X(S_{end})$, then the ESP goes into the inner space of (C_1) with the direction $\dot{\mathbf{p}}(s_X)$. As Ω is outside (C_1) , the ESP must pass the boundary of (C_1) . We denote \mathbf{H} as the passing point. Since \mathbf{X} can see \mathbf{H} , the part of the ESP connecting \mathbf{X} and \mathbf{H} is not the shortest path (as it is longer than $\overline{\mathbf{XH}}$). This leads to a contradiction with Lemma 1. Hence:

$$\mathbf{W} \in \partial\sigma_X(S_{end}) \quad (\text{A5})$$

In addition, if $\mathbf{W} \neq \mathbf{Y}$, then $\mathbf{W} \notin (\alpha)$. By using Corollary 1, we can confirm that the particle will move far away from (P_c) so it cannot reach Ω on (P_c) . Thus, $\mathbf{W} \equiv \mathbf{Y}$. (Q.E.D.)

iii. Case 3: $\mathbf{X} \in \mathbf{P3}$ (\mathbf{X} cannot see S_{end})

As \mathbf{X} cannot see S_{end} , there exists the farthest cross-section S_f of the tube that can be seen by \mathbf{X} . We will prove that \mathbf{X} can see only one point in this cross-section. In S_f , if there exist two different visible points \mathbf{Y}_1 and \mathbf{Y}_2 by \mathbf{X} , then \mathbf{X} can see the midpoint \mathbf{Y}_m of $\overline{\mathbf{Y}_1\mathbf{Y}_2}$ (using Lemma 2). As $\mathbf{Y}_m \notin \partial\Omega$, we infer that S_f is not the farthest visible cross-section by \mathbf{X} (\mathbf{X} can see farther with the line of sight through \mathbf{Y}_m). Thus, there is only one visible point \mathbf{Y} in S_f that can be seen by \mathbf{X} , and $\overline{\mathbf{XY}}$ is the correct direction of the tendon according to Corollary 2.

Moreover, we can demonstrate that $\overline{\mathbf{XY}}$ is also the longest-length-of-sight from \mathbf{X} . One can easily confirm that $\overline{\mathbf{XY}}$ must be tangent to $\partial\Omega$ at a point \mathbf{T} of the cross-section S_T . Let (α) be the corresponding tangent plane. Let Ω_v be the space enclosed by $\partial\Omega$, (α) , and the cross-section containing \mathbf{X} as illustrated in Fig. A2. Then, Ω_v contains all the visible points by \mathbf{X} of Ω located behind the cross-section S_T . The problem now is to prove that $\overline{\mathbf{XY}}$ is the longest length of sight in Ω_v . As the tube does not overlap itself, we obtain: $\overline{\mathbf{XY}} \geq \overline{\mathbf{TY}} \geq 2R$. Thus, one can confirm that Ω_v is totally contained by the sphere (χ) center \mathbf{X} and the radius $\overline{\mathbf{XY}}$. We then have $\overline{\mathbf{XY}}$ is the longest length of sight from \mathbf{X} . ^{c1}

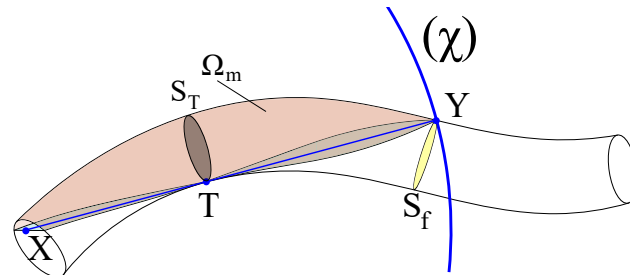


Figure A2. \mathbf{X} cannot see the ending cross-section. It can see only one point \mathbf{Y} on the furthest visible cross-section S_f .

^{c2}It is evident that every point on the ESP must belong to one of the three partitions (**P1**: see Ω , **P2**: see S_{end} , but not see Ω , and **P3**: not see S_{end}) and as the correct direction is unique for each position, if the VP follows the proposed correct direction throughout its journey, its moving path will describe the ESP. (Q.E.D.)

References

1. Li, F.; Klette, R. Euclidean shortest paths. In *Euclidean Shortest Paths*; Springer, 2011; pp. 3–29.
2. Özaslan, T.; Shen, S.; Mulgaonkar, Y.; Michael, N.; Kumar, V. Inspection of penstocks and featureless tunnel-like environments using micro UAVs. *Field and Service Robotics*. Springer, 2015, pp. 123–136.
3. Özaslan, T.; Mohta, K.; Keller, J.; Mulgaonkar, Y.; Taylor, C.J.; Kumar, V.; Wozencraft, J.M.; Hood, T. Towards fully autonomous visual inspection of dark featureless dam penstocks using MAVs. 2016 IEEE/RSJ International Conference on Intelligent Robots and Systems (IROS). IEEE, 2016, pp. 4998–5005.

^{c1} Remove text: (Q.E.D.)

^{c2} Text added.

4. Özaskan, T.; Loiano, G.; Keller, J.; Taylor, C.J.; Kumar, V.; Wozencraft, J.M.; Hood, T. Autonomous navigation and mapping for inspection of penstocks and tunnels with MAVs. *IEEE Robotics and Automation Letters* **2017**, *2*, 1740–1747. 470–472
5. Quenzel, J.; Nieuwenhuisen, M.; Droschel, D.; Beul, M.; Houben, S.; Behnke, S. Autonomous MAV-based indoor chimney inspection with 3D laser localization and textured surface reconstruction. *Journal of Intelligent & Robotic Systems* **2019**, *93*, 317–335. 473–475
6. Petrлік, M.; Báča, T.; Heřt, D.; Vrba, M.; Krajník, T.; Saska, M. A Robust UAV System for Operations in a Constrained Environment. *IEEE Robotics and Automation Letters* **2020**, *5*, 2169–2176. 476–478
7. Shukla, A.; Karki, H. Application of robotics in onshore oil and gas industry—A review Part I. *Robotics and Autonomous Systems* **2016**, *75*, 490–507. 479–480
8. Chataigner, F.; Cavestany, P.; Soler, M.; Rizzo, C.; Gonzalez, J.P.; Bosch, C.; Gibert, J.; Torrente, A.; Gomez, R.; Serrano, D. Arsi: an aerial robot for sewer inspection. In *Advances in Robotics Research: From Lab to Market*; Springer, 2020; pp. 249–274. 481–483
9. Tan, C.H.; Ng, M.; Shaiful, D.S.B.; Win, S.K.H.; Ang, W.; Yeung, S.K.; Lim, H.; Do, M.N.; Foong, S. A smart unmanned aerial vehicle (UAV) based imaging system for inspection of deep hazardous tunnels. *Water Practice & Technology* **2018**, *13*, 991–1000. 484–486
10. Tan, C.H.; bin Shaiful, D.S.; Ang, W.J.; Win, S.K.H.; Foong, S. Design optimization of sparse sensing array for extended aerial robot navigation in deep hazardous tunnels. *IEEE Robotics and Automation Letters* **2019**, *4*, 862–869. 487–489
11. Mallios, A.; Ridaio, P.; Ribas, D.; Carreras, M.; Camilli, R. Toward autonomous exploration in confined underwater environments. *Journal of Field Robotics* **2016**, *33*, 994–1012. 490–491
12. Fairfield, N.; Kantor, G.; Wettergreen, D. Real-time SLAM with octree evidence grids for exploration in underwater tunnels. *Journal of Field Robotics* **2007**, *24*, 03–21. 492–493
13. Gary, M.; Fairfield, N.; Stone, W.C.; Wettergreen, D.; Kantor, G.; Sharp, Jr, J.M. 3D Mapping and Characterization of Sistema Zacatón from DEPTHX (DE ep P hreatic TH ermal e X plorer). In *Sinkholes and the Engineering and Environmental Impacts of Karst*; 2008; pp. 202–212. 494–496
14. Pidic, A.; Aasbøe, E.; Almankaas, J.; Wulvik, A.; Steinert, M. Low-Cost Autonomous Underwater Vehicle (AUV) for Inspection of Water-Filled Tunnels During Operation. Proceedings of the, 2018. 497–499
15. Alvarez, A.; Caiti, A.; Onken, R. Evolutionary path planning for autonomous underwater vehicles in a variable ocean. *IEEE Journal of Oceanic Engineering* **2004**, *29*, 418–429. 500–501
16. Gao, X.Z.; Hou, Z.X.; Zhu, X.F.; Zhang, J.T.; Chen, X.Q. The shortest path planning for manoeuvres of UAV. *Acta Polytechnica Hungarica* **2013**, *10*, 221–239. 502–503
17. Dang, T.; Mascarich, F.; Khattak, S.; Nguyen, H.; Nguyen, H.; Hirsh, S.; Reinhart, R.; Papachristos, C.; Alexis, K. Autonomous search for underground mine rescue using aerial robots. 2020 IEEE Aerospace Conference. IEEE, 2020, pp. 1–8. 504–506
18. Petrлік, M.; Báča, T.; Heřt, D.; Vrba, M.; Krajník, T.; Saska, M. A robust uav system for operations in a constrained environment. *IEEE Robotics and Automation Letters* **2020**, *5*, 2169–2176. 507–508
19. Swaney, P.J.; York, P.A.; Gilbert, H.B.; Burgner-Kahrs, J.; Webster, R.J. Design, fabrication, and testing of a needle-sized wrist for surgical instruments. *Journal of medical devices* **2017**, *11*. 509–510
20. Nguyen, D.V.A.; Girerd, C.; Boyer, Q.; Rougeot, P.; Lehmann, O.; Tavernier, L.; Szewczyk, J.; Rabenoroso, K. A Hybrid Concentric Tube Robot for Cholesteatoma Laser Surgery. *IEEE Robotics and Automation Letters* **2022**, *7*, 462–469. 511–513
21. Canny, J.; Reif, J. New lower bound techniques for robot motion planning problems. 28th Annual Symposium on Foundations of Computer Science (sfcs 1987), 1987, pp. 49–60. 514–515
22. Sharir, A.; Baltsan, A. On shortest paths amidst convex polyhedra. Proceedings of the second annual symposium on Computational geometry, 1986, pp. 193–206. 516–517
23. Gewali, L.P.; Ntafos, S.; Tollis, I.G. Path planning in the presence of vertical obstacles. *IEEE Transactions on Robotics and Automation* **1990**, *6*, 331–341. 518–519
24. Agarwal, P.K.; Sharathkumar, R.; Yu, H. Approximate Euclidean shortest paths amid convex obstacles. Proceedings of the twentieth Annual ACM-SIAM Symposium on Discrete Algorithms. SIAM, 2009, pp. 283–292. 520–522
25. Mitchell, J.S.; et al. Geometric Shortest Paths and Network Optimization. *Handbook of computational geometry* **2000**, *334*, 633–702. 523–524
26. Deschamps, T.; Cohen, L.D. Fast extraction of minimal paths in 3D images and applications to virtual endoscopy. *Medical image analysis* **2001**, *5*, 281–299. 525–526
27. Bulow, T.; Klette, R. Digital curves in 3D space and a linear-time length estimation algorithm. *IEEE transactions on pattern analysis and machine intelligence* **2002**, *24*, 962–970. 527–528

28. Li, F.; Klette, R. Rubberband algorithms for solving various 2D or 3D shortest path problems. 2007 International Conference on Computing: Theory and Applications (ICCTA'07). IEEE, 2007, pp. 9–19. 529–531
29. Dogan, F.; Yayli, Y. On the curvatures of tubular surface with Bishop frame. *Communications Faculty of Sciences University of Ankara Series A1 Mathematics and Statistics* **2011**, *60*, 59–69. 532–533
30. Chow, S.N.; Lu, J.; Zhou, H.M. Finding the shortest path by evolving junctions on obstacle boundaries (E-JOB): An initial value ODEs approach. *Applied and Computational Harmonic Analysis* **2013**, *35*, 165–176. 534–536
31. Elmokadem, T.; Savkin, A.V. A method for autonomous collision-free navigation of a quadrotor UAV in unknown tunnel-like environments. *Robotica* **2021**, p. 1–27. 537–538
32. Moore, E.F. The shortest path through a maze. Proc. Int. Symp. Switching Theory, 1959, 1959, pp. 285–292. 539–540
33. Dijkstra, E.W.; et al. A note on two problems in connexion with graphs. *Numerische mathematik* **1959**, *1*, 269–271. 541–542
34. Savkin, A.V.; Hoy, M. Reactive and the shortest path navigation of a wheeled mobile robot in cluttered environments. *Robotica* **2013**, *31*, 323–330. 543–544
35. Hachour, O. The use of the 3D Smoothed parametric curve Path planning for Autonomous mobile robots. *International journal of systems applications, engineering & development* **2009**. 545–546
36. Blaga, P.A. On tubular surfaces in computer graphics. *Stud. Univ. Babeş-Bolyai Inform. L* **2005**, pp. 81–90. 547–548
37. Bose, P.; Maheshwari, A.; Shu, C.; Wuhler, S. A survey of geodesic paths on 3D surfaces. *Computational Geometry* **2011**, *44*, 486–498. 549–550
38. Rucker, D.C.; Webster III, R.J. Statics and dynamics of continuum robots with general tendon routing and external loading. *IEEE Transactions on Robotics* **2011**, *27*, 1033–1044. 551–552
39. Krivoshapko, S.N.; Ivanov, V.N. *Encyclopedia of analytical surfaces*; Springer, 2015. 553
40. Thangavelautham, J.; Robinson, M.S.; Tait, A.; McKinney, T.; Amidan, S.; Polak, A. Flying, hopping Pit-Bots for cave and lava tube exploration on the Moon and Mars. *arXiv preprint arXiv:1701.07799* **2017**. 554–556
41. am Ende, B. 3D mapping of underwater caves. *IEEE Computer Graphics and Applications* **2001**, *21*, 14–20. 557–558
42. Boyd, S.; Boyd, S.P.; Vandenberghe, L. *Convex optimization*; Cambridge university press, 2004. 559